

Computational understanding of distribution of temperature and velocity of airflow past a flat unglazed transpired solar collector

SP Panigrahi¹, SK Maharana²

**Mechanical Engineering, Christ University, Bangalore, India*

*** Aeronautical Engineering, Acharya Institute of Technology, Bangalore, India*

Corresponding author; SP Panigrahi

Date of Submission: 17-08-2018

Date of acceptance: 31-08-2018

I. INTRODUCTION

Unglazed transpired solar collectors (UTC's) are now a well- recognized solar air heater for heating outside air directly. They are key components in many engineering applications, such as in institutional and residential heating, industrial processes like sewage wastewater treatment, and food processing [Siwei Li et al., 2014]. They differ from conventional solar air collectors in that their southern wall or rooftop is replaced by a black perforated sheet that allows the collection of solar irradiation. Typically, they consist of a thin, black aluminum or galvanized steel cladding perforated by tiny holes, mounted onto a southward facing wall or roof top. Incident solar energy raises the temperature of the perforated cladding above the ambient temperature. As a consequence, outside air is heated when it is drawn through the perforations by a ventilation fan. The heated air is directed through an air gap located between the building wall and the absorber plate. The heated air is then used to feed fresh air into buildings and other applications.

The idea of replacing conventional building cladding with a system that generates electricity and heat is an area that, until recently, has received only limited attention although the potential energy and cost savings from integrated and optimized solar technologies are high [Athienitis et al., 2011]. Unglazed transpired solar collectors, known as UTCs, consist of dark porous metal sheets (flat or corrugated) installed as the exterior layer of the building facade with a narrow gap beneath it. The cladding absorbs solar radiation, thus heating up the suction fan-driven air flowing through the perforations. Corrugated UTCs can be integrated with photovoltaic systems, thereby generating electricity and heat, resulting in overall efficiencies that can be up to 70% [Bambara, 2012]. In UTC systems, the hot air is collected at the outlet and used either to preheat ventilation air, or as an input to heat pumps, thus satisfying a significant part of the building's heating, cooling, and hot water requirements [Athienitis et al., 2011].

The airflow in UTCs is primarily driven by mechanical fans, although the thermal buoyancy effects induced by the solar radiation falling on the plate and the incident atmospheric boundary layer create complex aerodynamic effects with impingement, separation, reattachment, etc. The Re for the airflow through the perforations is generally on the order of 103, while that of the wind flow over the plate is relatively high. Thus, the corresponding flow regime may span from laminar, transition state, to turbulent. Moreover, the low porosity (0.5–2 %) formed by scattered small perforations, results in a non-uniform flow distribution over the plate and creates complex local airflow patterns. These differ from the classical case of homogeneous suction (it has also been referred to as uniform or continuous suction in the literature), e.g. Iglisch (1944), Kay (1948) and Schlichting and Gersten (2000), in which the perforation spacing distance is within few millimetres and the vertical velocity is assumed constant at the plate surface, giving rise to the asymptotic solution for the velocity field.

From the literatures surveyed it was found that there is a sparse work carried out on the quantification of heat contents of the air. The computation of heat (in terms of the temperature rise of air inside the cavity) is carried out numerically for turbulent(Re is of the order of 10^6) and laminar(below $Re < 100$) using the uniform approach velocity which varies from 0 to 1 m/s and the suction velocity that varies from .045 m/s to 0.077 m/s. The simulated radiation flux on the unglazed transpired solar collector is also changed extensively. This was not amply found in the literatures and hence it has been taken up. The relationship between the temperature and the location, the flow velocity inside a cavity with the holes at the surface of the UTC, the quantification of the heat

carried into the thermally insulated cavity are studied through the analysis of the data obtained from the solver using the R studio, an open source statistical computing environment.

II. GOVERNING EQUATIONS OF FLOW

The mass, momentum, and energy conservation equations of the time-averaged equations can be written in a conservative form as follows:

Mass conservation equation:

$$\frac{\partial \rho}{\partial t} + \frac{\partial \rho u_i}{\partial x_i} = 0 \quad (1)$$

Momentum conservation equation:

$$\frac{\partial \rho u_i}{\partial t} + \frac{\partial (\rho u_i u_j + p \delta_{ij})}{\partial x_j} = \frac{\partial (\tau_{ij} - \rho \overline{u_i u_j})}{\partial x_j} \quad (2)$$

Energy conservation equation:

$$\frac{\partial (\rho \varepsilon)}{\partial t} + \frac{\partial (\rho \varepsilon u_i)}{\partial x_i} = \frac{\partial (\tau_{ij} u_j - \rho \overline{u_i u_j} u_j)}{\partial x_i} - \frac{\partial (q_i + C_p \rho \overline{u_i \theta})}{\partial x_i} + \frac{\partial}{\partial x_i} \left[\left(\mu_l + \frac{\mu_t}{\sigma_k} \right) \frac{\partial k}{\partial x_i} \right] \quad (3)$$

Turbulence Models

One of the turbulence models used in this research is k-ε. The description of which is outlined below.

In the case of Reynolds Averaged Navier-Stokes (RANS) equations, a Standard Turbulence Model (STM) such as the two-equation (k-ε) turbulence model is used:

$$\frac{\partial \rho k}{\partial t} + \frac{\partial \rho u_j k}{\partial x_j} = - \rho \overline{u_j u_j} \frac{\partial k}{\partial x_j} + \frac{\partial}{\partial x_j} \left[\left(\mu_l + \frac{C_\mu k^2}{\sigma_k \varepsilon} \right) \frac{\partial k}{\partial x_j} \right] - \rho \varepsilon (1 + M_\tau^2 M_\tau^2) \quad (4)$$

$$\frac{\partial \rho \varepsilon}{\partial t} + \frac{\partial \rho u_j \varepsilon}{\partial x_j} = - C_{\varepsilon 1} \rho \overline{u_j u_j} \frac{\varepsilon}{k} + \frac{\partial}{\partial x_j} \left[\left(\mu_l + \frac{C_\mu k^2}{\sigma_k \varepsilon} \right) \frac{\partial \varepsilon}{\partial x_j} \right] - f_2 f_2 \rho \overline{C_{\varepsilon 2} \varepsilon} \quad (5)$$

where

$$C_\mu = 0.09, C_{\varepsilon 1} = 1.44, C_{\varepsilon 2} = 1.44, \overline{\sigma_k \sigma_k} = \sigma_k \sigma_k = 1.4, \overline{\sigma_\varepsilon \sigma_\varepsilon} = \sigma_\varepsilon \sigma_\varepsilon = 1 \text{ and } \overline{C_{\varepsilon 2} C_{\varepsilon 2}} = C_{\varepsilon 2} C_{\varepsilon 2} = 1.92$$

$$f_\mu = f_\mu = \exp \left[\frac{-3.41}{(1 + \frac{R_T}{50})^2} \right] \left[\frac{-3.41}{(1 + \frac{R_T}{50})^2} \right]; R_T = \frac{k^2}{\mu_t^2} R_T = \frac{k^2}{\mu_t^2}; f_2 = f_2 = 1 - 0.3 \exp \left(-\frac{R_T^2}{R_T^2} \right)$$

Boundary conditions for epsilon (ε) and k at the wall are

$$\varepsilon_{\text{wall}} \varepsilon_{\text{wall}} = \nu_l \nu_l \left(\frac{\partial \sqrt{k}}{\partial n} \right)^2 \left(\frac{\partial \sqrt{k}}{\partial n} \right)^2; k_{\text{wall}} k_{\text{wall}} = 0$$

The turbulent stress components are

$$\rho \overline{u_j u_i} \rho \overline{u_j u_i} = 2 \rho \nu_t S_{ji} \rho \nu_t S_{ji} - \frac{22}{33} \delta_{ji} \delta_{ji} \rho k \quad \text{and}$$

$$S_{ji} S_{ji} = \frac{11}{22} \left[\frac{\partial u_j}{\partial x_i} + \frac{\partial u_i}{\partial x_j} \right] \left[\frac{\partial u_j}{\partial x_i} + \frac{\partial u_i}{\partial x_j} \right] - \frac{11}{33} \delta_{ji} \delta_{ji} \frac{\partial u_j \partial u_j}{\partial x_i \partial x_i}$$

III. METHODOLOGY

In this section the work done on flat unglazed transpired solar collector (UTC) is presented. The geometry used for the simulation of flow and heat transfer is shown in **Fig.1 (a)**. In the region above the plate, the left side of the domain was defined as the velocity-inlet with a specified approaching flow velocity and the right side of the domain was defined as the pressure-outlet with zero gauge pressure. The plate was set to be a wall with thickness of 0.00086m and the perforations on the plate were set to be ‘interior’. The bottom of the cavity was defined as velocity-outlet with a specified suction velocity. The left and right side of the cavity were defined as adiabatic walls. A symmetry boundary condition was used for all other faces, which means zero velocity and temperature gradient. The upper domain is 0.3m height, which is sufficient for the boundary layer growth. The plate is divided into two parts in the stream-wise direction: a perforation row and a solid row. The perforation row includes all the perforations and can be considered as a ‘discrete suction’ component. The solid row covers more than 90% of the plate area and it is similar to a smooth, impermeable flat plate, but the flow is different from the classical flat plate case due to the suction created by the perforation row. A perforated plate with an area of 0.6m x 0.6m and a cavity with 0.15m height were considered. The plate has pitch length of

0.01689 m and perforation diameter of 0.00159 m. The simulated solar radiation in the experiments was around 600W/m^2 , the ambient air temperature 298K, and the turbulence intensity of incoming flow 1%, which is considered to be uniform. These values were used as inputs in the CFD model.

The Standard $k-\epsilon$, Shear Stress Transport $k-\omega$ (SST $k-\omega$) turbulence closure models and Laminar model available in ANSYS were applied to a 3-dimensional computational domain. A second order upwind scheme was adopted for all the variables except pressure. The discretization of pressure is based on a staggered scheme. The SIMPLE algorithm was used to couple the pressure and momentum equations. If the sum of absolute normalized residuals for all the cells in flow domain became less than 10^{-6} for all variables, the solution was considered converged. In all simulations, the $y+$ value is maintained around 1 to satisfy the enhanced wall treatment requirement.

The grid independence for each case was verified using three different grids to ensure that grid resolution would not have a notable impact on the results. The results of the grid independence study are listed below in Table 1.

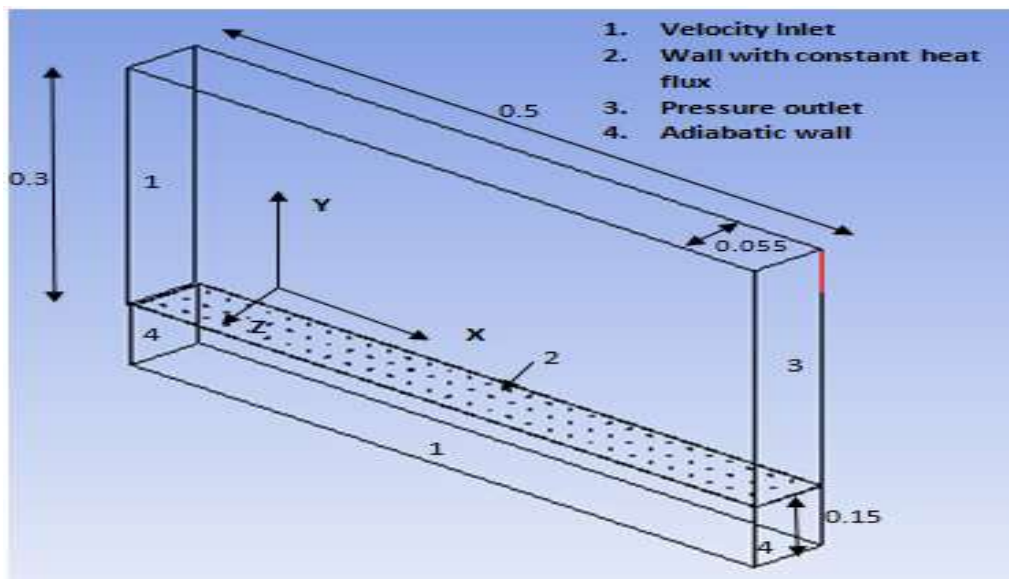


Fig.1 (a) Flat UTC model configuration (unit: m) – Computational Domain

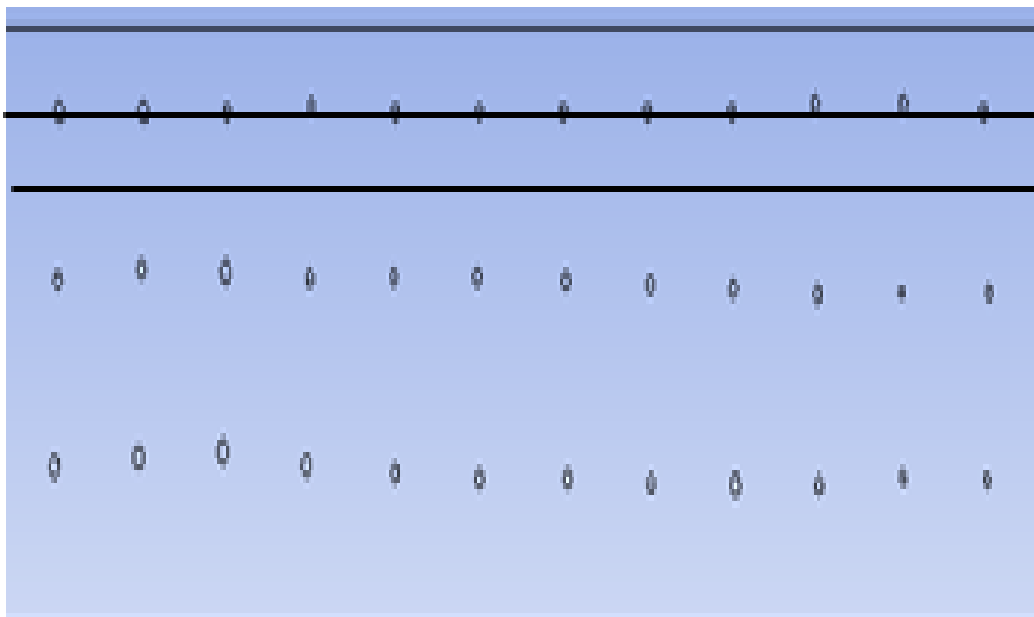


Fig.1 (b) Sketch of perforated and solid rows

The plate has pitch length of 16.89 mm and a perforation diameter of 1.59 mm. The simulated solar radiation is 600 W/m². The ambient temperature 298K and the uniform 1% turbulence intensity of the oncoming flow were used as the inputs for CFD model. The simulated approach flow velocity ranges from 0 to 1 m/s and the suction velocity spans from 0.045 to 0.077 m/s, which were the tested conditions in the experiments.

In the region above the plate, the left side of the domain was defined as the ‘velocity inlet’ with a specified approach flow velocity and the right side of the domain was defined as the ‘pressure outlet’ with zero gauge pressure. The plate was set to be a wall with heat flux of 600 W/m² and thickness of 0.86 mm and the perforations on the plate were set to be ‘interior’. The bottom of the cavity was also defined as a ‘velocity inlet’, but with reversed flow direction and a specified suction velocity. The left and right side of the cavity were defined as adiabatic walls. A symmetry boundary condition was used for all other faces, enforcing zero velocity and temperature gradients. The upper domain is 0.3 m height, which is sufficiently high to not affect the boundary layer growth along the collector surface and to eliminate any possible influence due to the size of the computational domain.

Boundary Condition

Boundary conditions used for the simulation of flow and heat transfer are shown in the Fig.2.

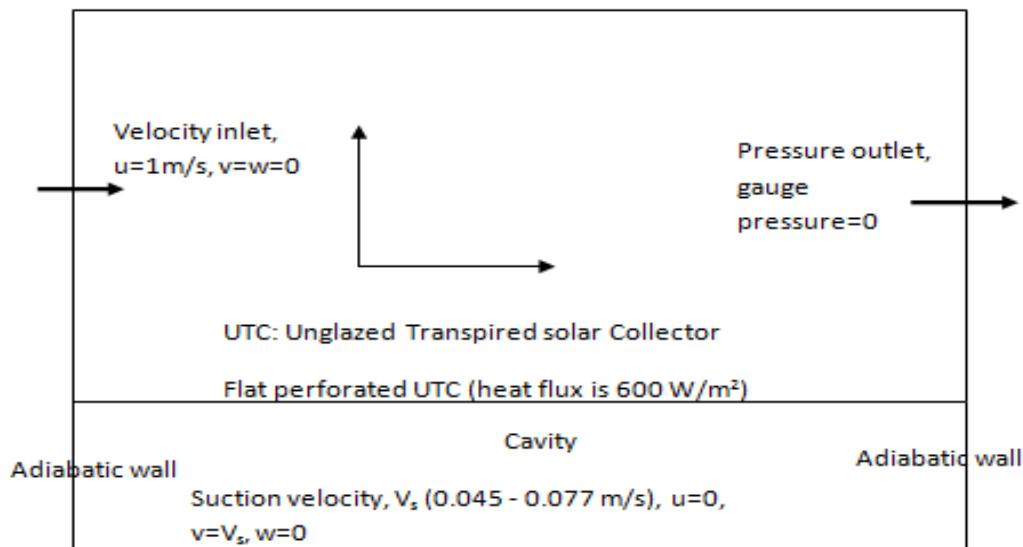


Fig.2 Schematic diagram with boundary condition for the flow domain in X-Y plane

Convergence and mesh independence study

The convergence of the numerical solutions obtained from the above-mentioned problem is obtained by the residuals of the values of variables. In this work, convergence occurs when the values of total residual become smaller than 10⁻⁶. All these values have reached their acceptable steady solutions during the simulation. The solutions are also independent of the mesh resolution. The grid independence for each case was verified using three different grids to ensure that grid resolution would not have a notable impact on the results. The results of the grid independence study are listed below in Table 1.

Table 1: Grid Independence Study

Plate temperature / Cavity outlet temperature [K]	Cell numbers			Experimental data
	Grid 1 (286000)	Grid 2 (200000)	Grid 3 (135000)	
Case 1: wind speed=1m/s, suction velocity=0.077m/s	314.0/305.9	314.5/305.7	314.7/305.0	313.9/306.5
Case 2: wind speed=1m/s, suction velocity=0.045m/s	315.4/307.	314.8/307.1	313.7/306.9	313.9/306.5

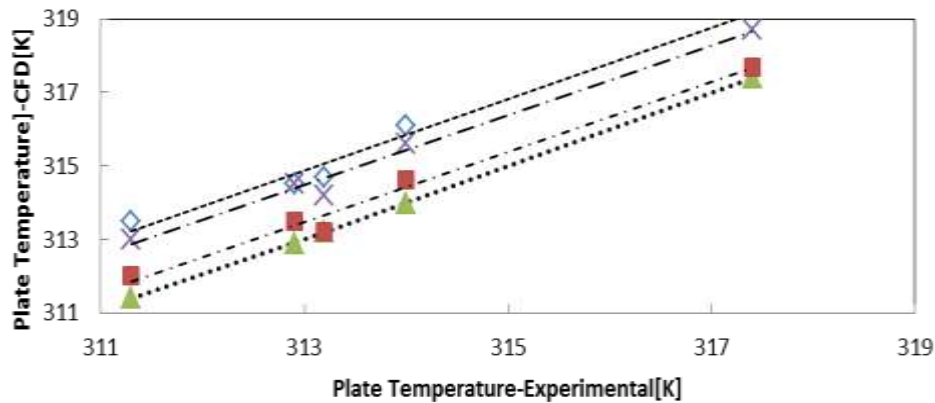
IV. RESULTS AND DISCUSSIONS

The tested cases are listed in **Table 2**. The average plate surface temperature and cavity outlet temperature computed using different RANS models are compared with the experimental data and the results are shown in **Fig.3 (a)-(b)**.

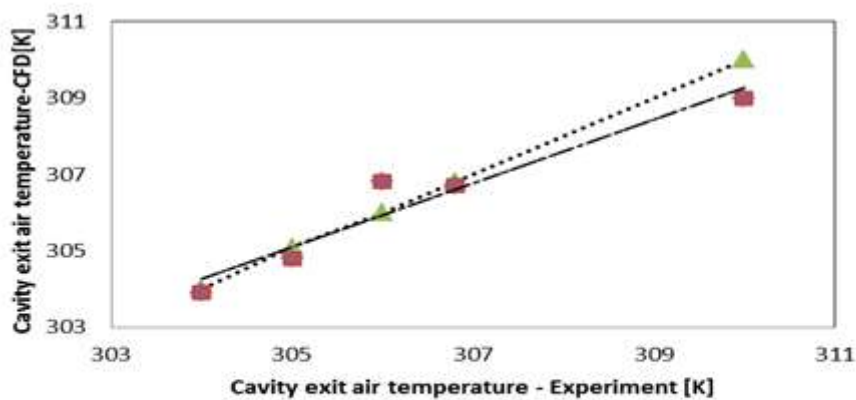
Table 2 : Tested cases for model validation

Cases	1	2
Wind Speed[m/s]	1	1
Suction Velocity [m/s]	.045	.077

For the plate surface temperature, the agreement between CFD results and experimental data is satisfactory. The standard k-ε model is more stable in terms of convergence and more consistent. The performance of the SST k-ω model and laminar is different than all the k-ε models with the results showing that surface temperature is overestimated. For the cavity outlet temperature, all models provided identical results. Thus, based on this comparison, the standard k-ε can provide sufficiently accurate results for thermal modeling, however, the standard k-ε model was adopted for the parametric study due to its slightly lower computing time and better convergence process. The laminar and SST k-ω are also considered for comparison purpose.



(a)



(b)

Fig.3 Comparison between CFD results and experimental data from the literature for flat UTC model: (a) plate surface temperature and (b) cavity exit air temperature.

From the **Fig. 4** it is observed that the mean y-component of velocity predicted by k-ε turbulence model is more chaotic in the cavity zone compared to that predicted by k-ω turbulence model . The velocity variation is predictable and follows a pattern in case of k-ω. The **Fig.5** shows a comparison of velocity profile, U_y of air within the chamber predicted by 3 different models k-ω , laminar and k-ε for suction velocity, $V_s=0.077$ m/s . Although the variations by all the three models look similar, at $Y=0.011$, the higher value of U_y is predicted by the Laminar model. It supersedes k-ε and k-ω which predicts the lowest value. Between $Y=0.21$ and 0.31 (middle of the cavity) the U_y predicted by all models rises sharply and remains almost the same. From $Y=0.31$ to 0.51 , the U_y rises. This change of variation is due to the inherent nature of the flow near the walls (velocity component is towards lowest value) friction deters the growth of velocity and near the surface of UTC (perforated one) the speed is hugely affected by the suction velocity and it adds to increase the magnitude of U_y . The temperatures predicted [shown in **Fig.6**] by laminar model are higher than that predicted by other two turbulence models in the region indicated by $Y=0.31$ to 0.5 . For the suction velocity $V_s=0.077$ m/s, the cavity exit air temperature is rising from 298 K to 318.2 K . For suction velocity $V_s=0.045$ m/s, the plate temperatures predicted by all three models start rising from 302 K. The highest value of the temperature predicted by the Laminar model is 348 K.

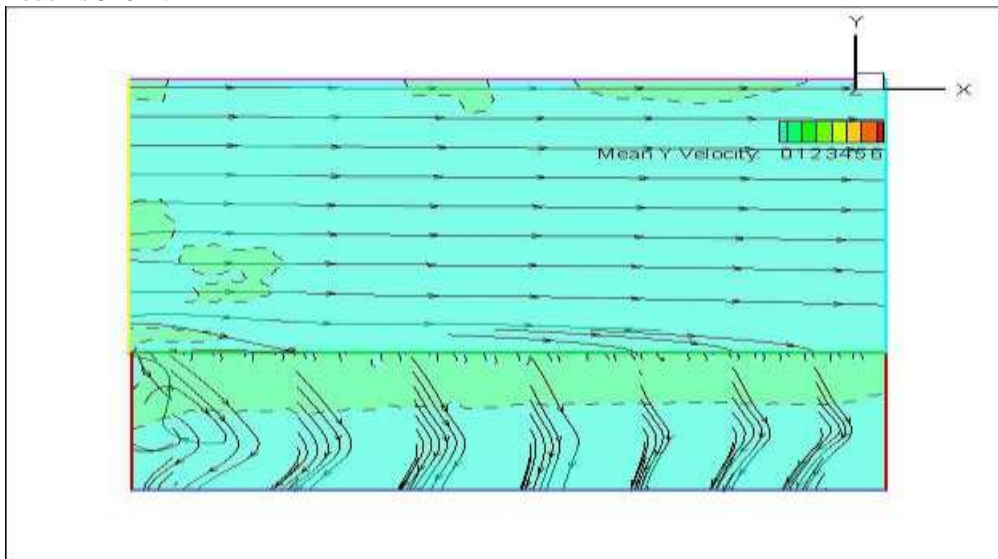


Fig. 4 Mean U_y velocity and pathlines in the cavity predicted by CFD [k-ω]

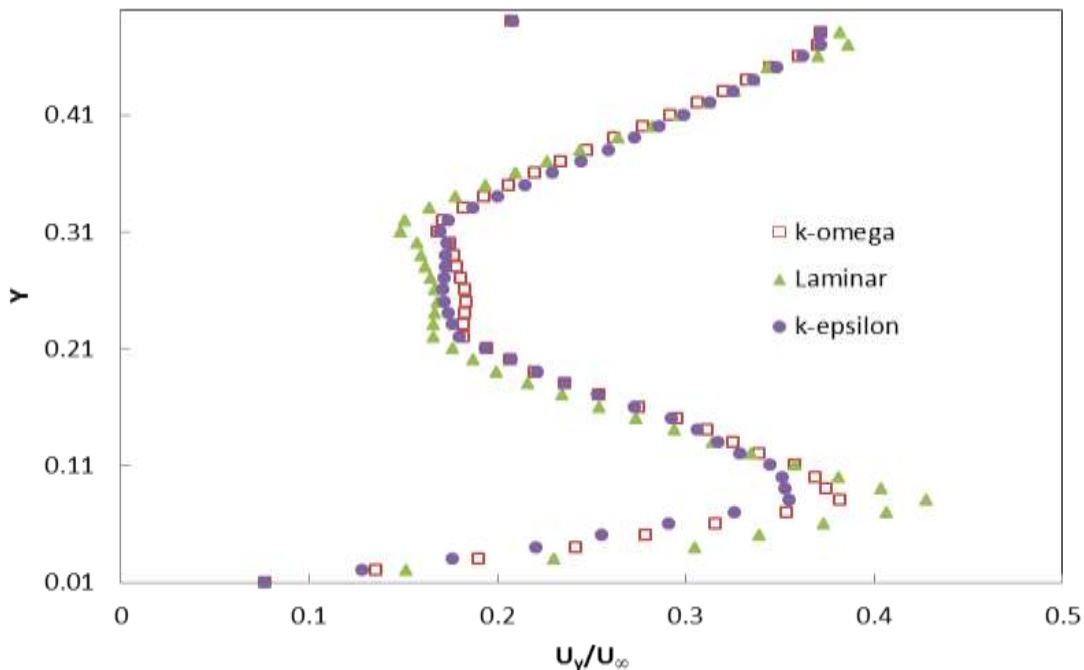


Fig.5 Comparison of velocity profile, U_y of hot air within the chamber predicted by 3 different models k-ω , Laminar and k-ε for suction velocity, $V_s=0.077$ m/s

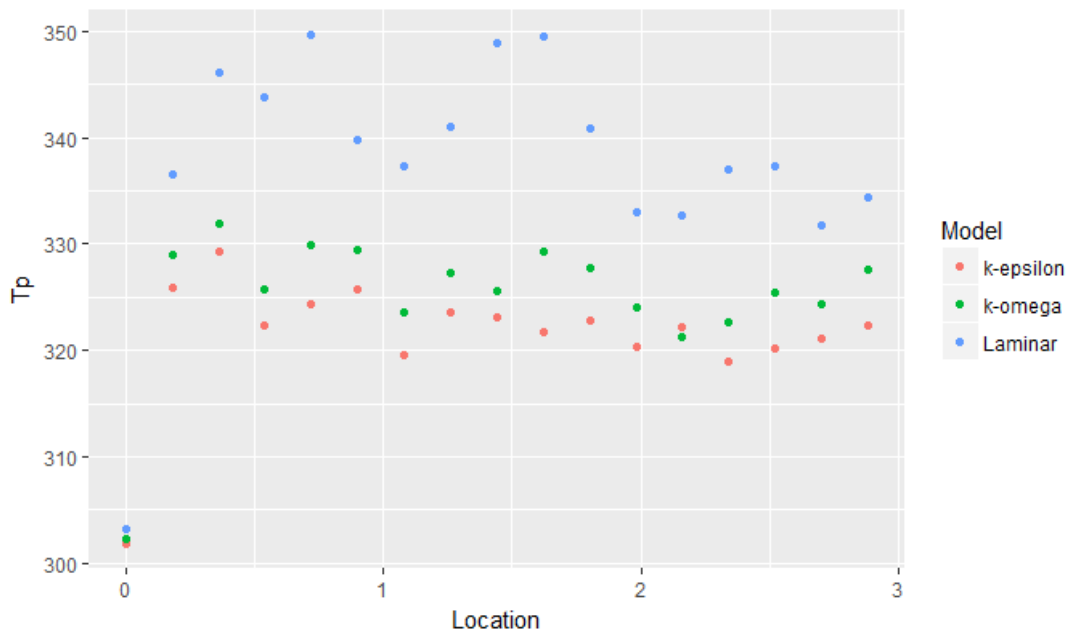


Fig.6 Comparison of Plate Temperatures predicted by 3 different models k- ω (k-omega), Laminar and k- ϵ (k-epsilon) for suction velocity, $V_s = 0.077$ m/s

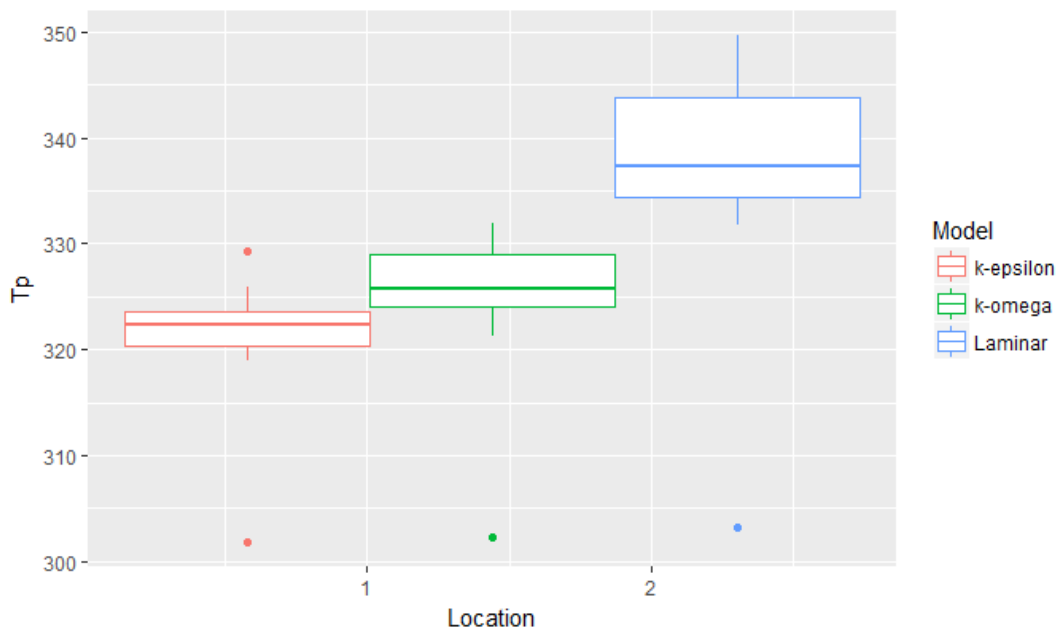


Fig.7 Box plots to show the range and characteristics of plate temperatures predicted by 3 different models k- ω (k-omega), Laminar and k- ϵ (k-epsilon) for suction velocity, $V_s = 0.077$ m/s

The Fig.7 is showing the range and characteristics of plate temperatures predicted by 3 different models k- ω (k-omega), laminar and k- ϵ (k-epsilon) for suction velocity, $V_s = 0.077$ m/s . This is a very good way of knowing the growth of plate temperature for different flow condition. In this case the laminar flow could develop a good amount of heat for the air that goes into the cavity.

A simple linear regression analysis was done to see if there is any linear relationship between the exit temperature (a target) and location of the hole (a predictor). The scatter plot shown in Fig.8 shows the distribution of Fitted values vs residuals(errors). The outliers in this plot are labelled by their observation number. In this case the outliers are labelled as 1, 2 and 3. The model fits linearly well . Whereas the model does not linearly fit for plate temperature vs location plot. There are outliers and non-linearity effects are evident in Fig. 9.

Residual vs Fitted values:

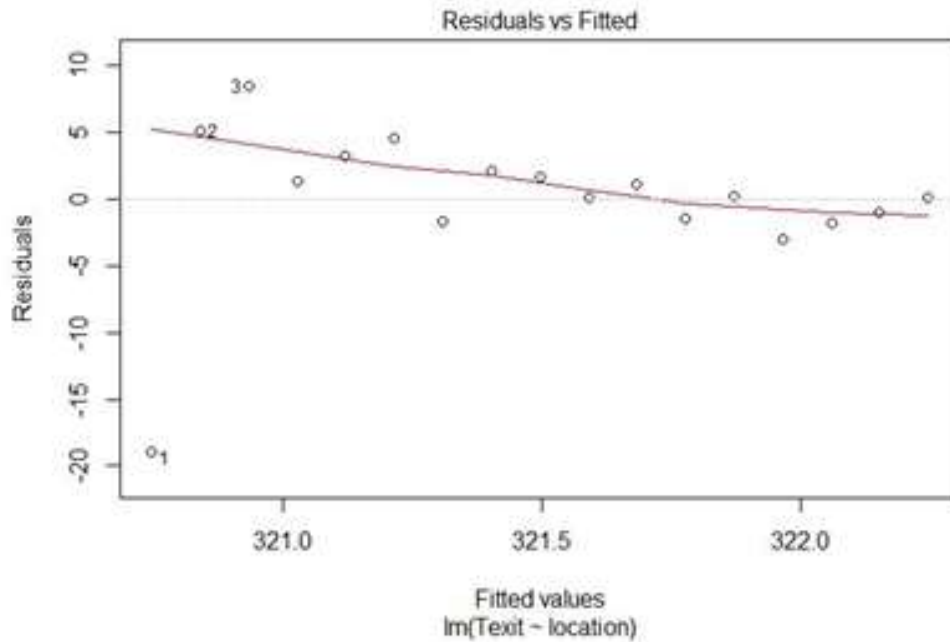


Fig. 8 Scatter plot for the distribution of Texit (Fitted value) vs location(a predictor)

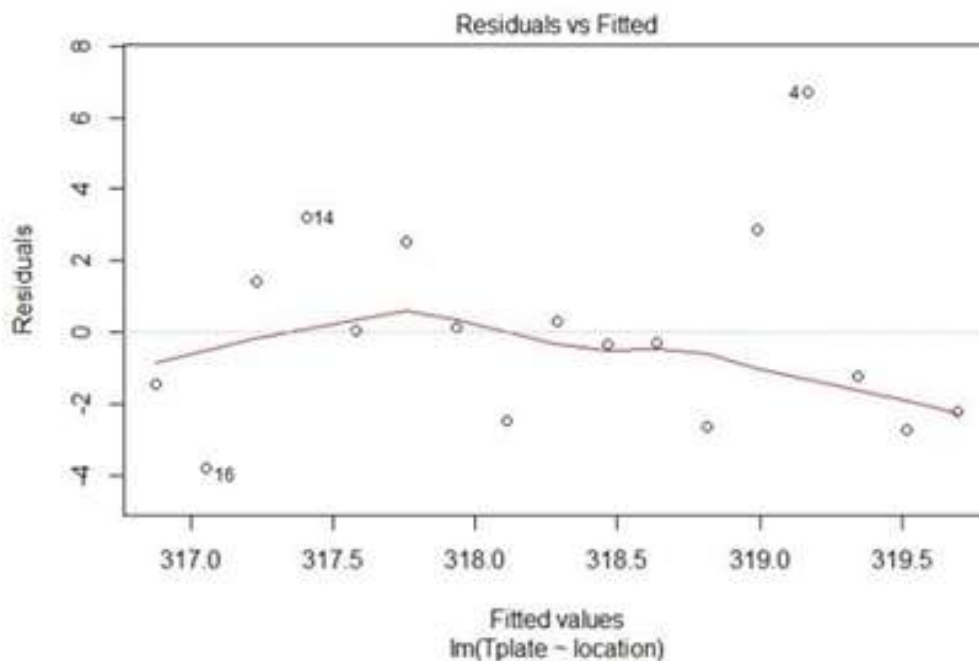


Fig. 9 Scatter plot for the distribution of plate temperature (Fitted value) vs location(a predictor)

The Fig. 10 is a residual vs fitted plot. Around the residual =0 the fitted values are varying so much and hence they are not well behaved and a non-linear relationship exists between the V_y and location of the hole.

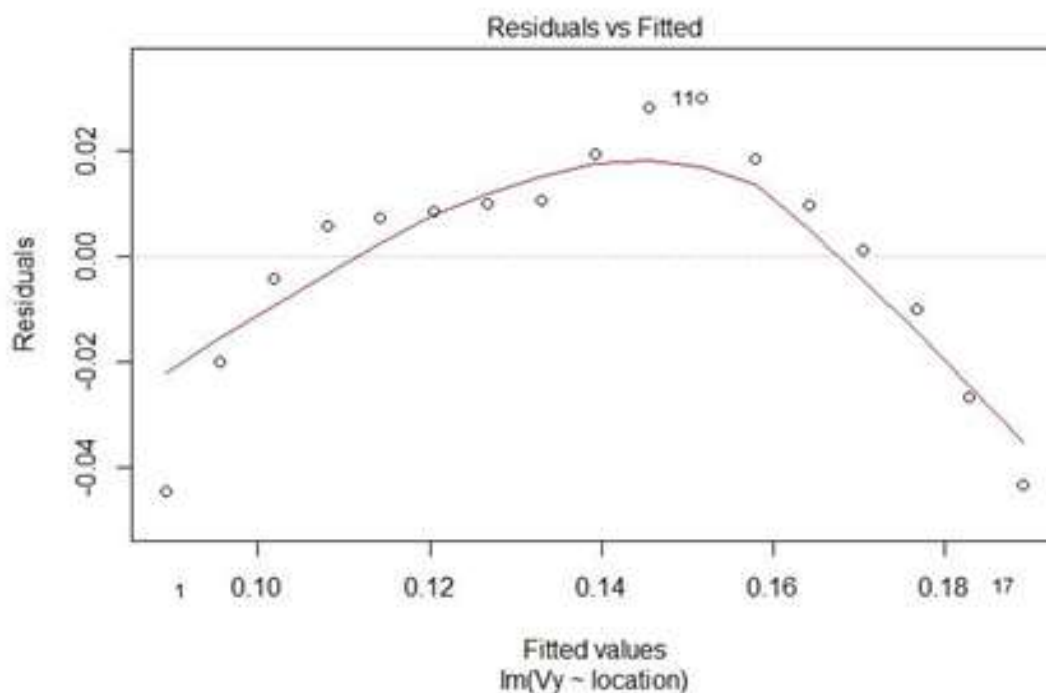


Fig. 10 Scatter plot for the distribution of mean Y- velocity (Fitted value) vs location(a predictor)

V. CONCLUSION

The numerical simulation of fluid flow and heat transfer through a perforated flat UTC was carried out. The validation of the results with the experimental data was satisfactory. There was 5% difference between the two comparisons which could be accepted as the numerical inaccuracies and the limit of very fine grid are constraints to an accurate match. The rise of plate temperature and cavity air exit temperature was also studied for two suction velocities ($V_s=0.045$ m/s and 0.077 m/s). For $V_s=0.045$ m/s and Laminar model the temperature rise of the plate is 30% higher than the values predicted by taking $V_s=0.077$ m/s and k- ϵ and k- ω models. The data analysis and linear regression predicted that the plate temperature ranges 30% higher for a laminar flow situation than that of other two turbulent flow conditions. The linear regression predicted that the V_y has non-linear relationship with the location of the holes in UTC. The exit temperature has linear relationship with location.

REFERENCES

- [1]. Cristiana V. Croitoru, Ilinca Nastase, Florin I. Bode, Amina Meslem, Thermodynamic investigation on an innovative unglazed transpired solar collector, ELSEVIER, Solar Energy, Solar Energy 131 (2016) 21–29
- [2]. Roozbeh Vaziri, M. Ilkan, F. Egelioglu, Experimental performance of perforated glazed solar air heaters and unglazed transpired solar air heater, ELSEVIER, Solar Energy Volume Solar Energy 119 (2015) 251–260
- [3]. Siwei Li, Panagiota Karava, Sam Currie, William E. Lin, Eric Savory, Energy modeling of photovoltaic thermal systems with corrugated unglazed transpired solar collectors – Part 1: Model development and validation, ELSEVIER, Solar Energy 102 (2014) 282–296
- [4]. Siwei Li, Panagiota Karava, Sam Currie, William E. Lin, Eric Savory, Energy modeling of photovoltaic thermal systems with corrugated unglazed transpired solar collectors – Part 2: Performance analysis, ELSEVIER, Solar Energy 102 (2014) 297–307
- [5]. Michael R. Collins, Hani Abulkhair, An evaluation of heat transfer and effectiveness for unglazed transpired solar air heaters, ELSEVIER, Solar Energy 99 (2014) 231–245
- [6]. Siwei Li, Panagiota Karava, Eric Savory, William E. Lin, Airflow and thermal analysis of flat and corrugated unglazed transpired solar collectors, ELSEVIER, Solar Energy 91 (2013), 297–315
- [7]. Messaoud Badache, Daniel R. Rousse, Stéphane Hallé, Guillermo Quesada, Guillermo Quesada, Experimental and numerical simulation of a two-dimensional unglazed transpired solar air collector, ELSEVIER, Solar Energy 93 (2013) 209–219
- [8]. Siwei Li, Panagiota Karava, Evaluation of turbulence models for airflow and heat transfer prediction in BIPV/T systems optimization, ELSEVIER, Energy Procedia 30 (2012) 1025–1034
- [9]. Arulanandam, S.J., Hollands, K.G.T., Brundrett, E., A CFD heat transfer analysis of the transpired solar collector under no-wind condition. Solar Energy 67(1999.), 93–100.
- [10]. Athienitis, A.K., Bambara, J., O’Neill, B., Faille, J., A prototype photovoltaic/thermal system integrated with transpired collector. Solar Energy 85(2011) 139–153.

- [11]. Gawlik, K.M., A numerical and experimental investigation of heat transfer issues in the practical utilization of unglazed, transpired solar air heaters. Ph.D. Thesis(1993), Department of Civil, Environmental, and Architectural Engineering, University of Colorado, Colorado, USA.
- [12]. Iglisch, R., Exact calculation of laminar boundary layer in longitudinal flow over a flat plate with homogeneous suction. Schriften der Deutschen Akademie der Luftfahrtforschung, Band 8B, Heft 1. Translation: NACA TM No. 1205

SP Panigrahi "Computational understanding of distribution of temperature and velocity of airflow past a flat unglazed transpired solar collector "International Journal Of Modern Engineering Research (IJMER), vol. 08, no. 08, 2018, pp.46-55